

NANO EXPRESS

Open Access

Silver(I)-directed growth of metal-organic complex nanocrystals with bidentate ligands of hydroquinine anthraquinone-1,4-diyl diethers as linkers at the water-chloroform interface

Ying Tang¹, Hui-Ting Wang¹, Meng Chen¹, Dong-Jin Qian^{1*}, Li Zhang² and Minghua Liu²

Abstract

Immiscible liquid-liquid interfaces provide unique double phase regions for the design and construction of nanoscale materials. Here, we reported Ag(I)-directed growth of metal-organic complex nanocrystals by using AgNO_3 as a connector in the aqueous solution and bidentate ligand of 1,4-bis(9-O-dihydroquininyl)anthraquinone $[(\text{DHQ})_2\text{AQN}]$ and its enantiomer of $(\text{DHQD})_2\text{AQN}$ in the chloroform solutions as linkers. The $\text{Ag}-(\text{DHQ})_2\text{AQN}$ and $\text{Ag}-(\text{DHQD})_2\text{AQN}$ complex nanocrystals were formed at the liquid-liquid interfaces and characterized by using UV-vis absorption and fluorescence spectroscopy and X-ray photoelectron spectroscopy, as well as by using scanning electron microscopy. Screw-like nanocrystals were formed at the initial 30 min after the interfacial coordination reaction started, then they grew into nanorods after several days, and finally became cubic microcrystals after 2 weeks. The pure ligand showed two emission bands centered at about 363 and 522 nm in the methanol solution, the second one of which was quenched and shifted to about 470 nm in the Ag-complex nanocrystals. Two couples of reversible redox waves were recorded for the Ag-complex nanocrystals; one centered at about -0.25 V (vs. Ag/AgCl) was designated to one electron transfer process of $\text{Ag} - (\text{DHQ})_2\text{AQN}$ and $\text{Ag} - (\text{DHQ})_2\text{AQN}^+$, and the other one centered at about 0.2 V was designated to one electron transfer process of $\text{Ag} - (\text{DHQ})_2\text{AQN}$ and $\text{Ag}^+ - (\text{DHQ})_2\text{AQN}$.

Keywords: Metal-organic complex nanocrystal; Liquid-liquid interface; Morphology; Fluorescence; Electrochemistry

Background

Self-assembly of nanostructural materials at the fluid interfaces has recently received growing attention because the interface regions have a double phase thickness of tens of nanometers depending on the nature of the solvents and species within them, a dimension of which is comparable to that of the nanostructural materials [1]. That is, the fluid interface provides a unique region for the growth of micro- or nanoscale materials and for the constrained chemical reactions [2,3]. It has been further found that those materials produced at the fluid interfaces are highly mobile and can rapidly achieve an equilibrium assembly with the reactants in each phase. The dynamic process of species or particles across interface

usually dominate composition, morphology, and structure of the materials produced [4,5]. The rapid diffusion of nanoparticles and reagents in either fluid phase leads to very efficient interfacial chemistry, including interfacial chemical reactions and molecular assembly.

Immiscible solutions are often used to form the fluid interface since such an interface can provide a defect-free junction that has an importance for the products with high purity [6]. Many one-dimensional (1D) nanowires and nanotubes and 2D nanosheets and nanocombs of metals, metal oxide, metal sulfide, and complexes have been designed and constructed in the past decades [7-9]. Our previous work has revealed that the specific features of the metal ions (such as the geometry) and coordination numbers of the anionic ions or ligands take an important role in governing the crystal structure of the products [10-12], though a complex interplay of van der Waals,

* Correspondence: djqian@fudan.edu.cn

¹Department of Chemistry, Fudan University, 220 Handan Road, Shanghai 200433, China

Full list of author information is available at the end of the article

electrostatic, magnetic, molecular, and entropic effects needs to be considered. Besides the inorganic compounds, polymer crystalline nanomaterials could also be constructed at the liquid/liquid interfaces. For instance, Matsui and coworkers synthesized single crystalline conducting polymer, poly(3,4-ethylenedioxythiophene), with the fast conductance switching property [13]. They further prepared single crystalline nanoneedles of polyaniline and polypyrrole via an interfacial polymerization induced by FeCl_3 [14]; the products have a fast conductance switching time between the insulating and conducting states in the order of milliseconds.

Layered porous poly(4-vinylpyridine) (P4VP) films could also be formed at the water-oil interfaces with the porous diameters in the range from hundred nanometers to several micrometers [15]. Liu and coworkers have further developed this method to prepare microcapsules and foam films, which were used as platforms to form various composite inorganic nanomaterials. Examples included gold nanoparticle-doped poly(2-vinylpyridine) and poly(N-vinylcarbazole) composites [16,17] and silver- or gold-doped diblock copolymer of poly(t-butyl methacrylate)-block-poly(2-vinyl pyridine) composites [18]. These metal-doped composites showed high catalytic activity and durability on the reduction of organic compounds such as nitrobenzene, 4-nitrophenol, and 4-nitrobenzoic acid [19].

In the present work, Ag(I)-directed metal-organic complex nanocrystals were fabricated at the water-chloroform interface by using AgNO_3 as a connector and bidentate chiral ligand of 1,4-bis(9-O-dihydroquininyl)anthraquinone [(DHQ)₂AQN] and its enantiomer of (DHQD)₂AQN as linkers. Our previous work has revealed that AgNO_3 could direct formation of chiral coordination polymers (CPs) at the air-water interface [20]. Atomic force microscopic (AFM) images for the transferred CPs revealed irregular aggregates that were composed of many round particles. These particles were connected together to form wires with particular orientation. However, due to the limitation of the reaction species within the Langmuir monolayers at the air-water interface, the orientation of those aggregates was not clear. Hence, to clarify morphologies of these aggregates, the coordination reaction was performed here at the water-chloroform interface wherein the irregular aggregates may grow into relatively larger macro-/nanocrystals since there were enough inorganic metal ions and ligands in each phase. The as-prepared Ag-organic complex nanocrystals were characterized by using UV-vis absorption spectroscopy and X-ray photoelectron spectroscopy (XPS) and scanning electron microscopy (SEM). Finally, the luminescent behaviors and electrochemical properties of the nanocrystals were investigated.

Methods

Materials

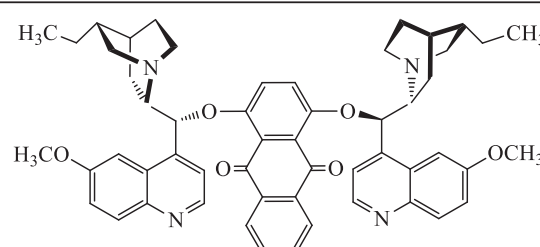
Chiral ligand of hydroquinine anthraquinone-1,4-diyl diether of (DHQ)₂AQN and its enantiomer (DHQD)₂AQN (Figure 1) were purchased from Sigma-Aldrich Co. (St. Louis, MO, USA). Chloroform was from Alfa Aesar[®] (Beijing, China). AgNO_3 was from Shanghai Chemical Reagent Co. (Shanghai, China). All chemicals were used as received without further purification. Ultrapure water (18.2 $\Omega\text{M cm}$) was prepared with a RephiLe filtration unit (RephiLe Bioscience Ltd, Shanghai, China).

Growth of Ag-complex nanocrystals at the water-chloroform interface

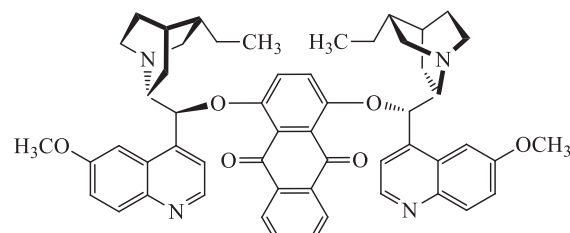
Interfacial self-assembly of the Ag-(DHQ)₂AQN or Ag-(DHQD)₂AQN complex nanocrystals was performed as follows: 20 mL 10 mM AgNO_3 aqueous solution was slowly added onto the surface of 30 mL (DHQ)₂AQN or (DHQD)₂AQN chloroform solution in a beaker. The reaction system was left undisturbed at room temperature from several minutes to 2 weeks. As a control experiment, interfacial phenomenon of (DHQ)₂AQN or (DHQD)₂AQN at the interface of pure water and ligand chloroform solution was also investigated.

Transfer of Ag-complex nanocrystals onto substrate surfaces

Layers of Ag-(DHQ)₂AQN or Ag-(DHQD)₂AQN complex nanocrystals grown at the interface were transferred onto substrate surfaces with the use of a dipper from



(DHQ)₂ANQ



(DHQD)₂ANQ

Figure 1 Structure of the ligands used in the present work.

KSV 5000 minitrough (KSV Instrument Co., Helsinki, Finland) or from JML04C2 trough (Powereach, Shanghai, China). The substrate was firstly immersed into the liquid-liquid interface before the interfacial reaction started, and after a given time waiting for the coordination reaction and formation of Ag-complex nanocrystals, the substrate was vertically withdrawn from the interface. The dipping rate was kept at 1 mm/min.

Instruments

UV-vis spectra were measured with the use of a Shimadzu UV-2550 UV-vis spectrophotometer (Shimadzu, Kyoto, Japan). Steady-state fluorescence spectra were recorded by using a Shimadzu RF-5300PC spectrophotometer.

XPS spectra were recorded by using a VG ESCALAB MKII multifunction spectrometer (VG Scientific, East Grinstead, UK), with nonmonochromatized Mg-K α X-rays as the excitation source. The system was carefully calibrated by Fermi edge of nickel, Au 4f_{2/7}, and Cu 2p_{2/3} binding energy. Pass energy of 70 eV and step size of 1 eV were chosen when taking spectra. In the analysis, chamber pressures of $1 \sim 2 \times 10^{-7}$ Pa were routinely maintained. The binding energies obtained in the XPS analysis were corrected by referencing the C1s peak to 284.60 eV.

Scanning electron microscopic (SEM) measurements were performed on a Philips XL30 electron microscope (Philips, Amsterdam, The Netherlands). The samples were deposited on the Si substrate surface. High-resolution transmission electron microscope image was acquired on a JEOL JEM-2010 transmission electron microscope (JEOL Ltd., Akishima-shi, Japan) operating at an accelerating voltage of 200 kV. The sample was deposited onto a 230-mesh copper grid covered with Formvar.

Cyclic voltammogram (CV) was measured by using an electrochemical analyzer (CHI 601b, CH Instruments, Inc., Shanghai, China). A Pt wire and Ag/AgCl electrode were used as the auxiliary and reference electrodes, respectively, and the indium tin oxide (ITO) electrode covered with layers of Ag-(DHQ)₂AQN or Ag-(DHQD)₂AQN nanocrystals was used as the working electrode with a 10 mmol/L HClO₄ solution as the electrolyte. For the CV measurement of the ligand redox reaction, an initial potential of -0.5 V was applied for 2 s, followed by cyclic scans to a final potential of 0 V. For the measurement of the Ag(I) redox reaction, the initial potential of -0.1 V was applied for 2 s, followed by cyclic scans to the final potential of 0.5 V. All CV measurements were done for 10 cycles under an Ar atmosphere at room temperature.

Results and discussion

Growth of Ag-complex nanocrystals at the water-chloroform interface

Interfacial reaction between the silver ion and ligand of (DHQ)₂AQN or (DHQD)₂AQN occurred quickly. During

experiments, we found that the reaction rate was closely dependent on the concentration of AgNO₃ in water and that of the ligand in chloroform as well as the temperature. Similar to those reported in the literature [21], stronger concentration of the reactants and higher reaction temperature could result in a quick formation of metal-organic complex nanocrystals. These nanocrystals were then transferred on various substrate surfaces by the vertical dipping method for the characterization of morphologies, absorption and emission spectra, XPS, and electrochemistry.

Morphology characterization

Morphologies of the Ag-directed complex nanocrystals were characterized by using SEM technique. These nanocrystals were deposited on the freshly cleaned Si substrate surface by vertical dipping method. Similar morphologies were obtained for the two ligands, so as an example, Figure 2 shows several SEM images of the Ag-(DHQ)₂AQN complex nanocrystals formed at the water-chloroform interface from the initial 5 min to 2 weeks, which revealed the following features.

Firstly, many screw-like nanocrystals were formed at the initial 30 min with a length of several hundred nanometers and diameters of tens of nanometers (Figure 2A,B). These nanocrystals formed aggregates possibly due to a strong interaction between each screw-like nanocrystal. Such kind of interactions between adjacent nanocrystals has been used to control the growth of large-scale or colloidal nanocrystal building blocks in the organic solutions [22]. As it has been reported that each silver ion may coordinate with two pyridyl groups [20,23], so we may suggest that each silver ion coordinated with two ligands to form Ag-directed CP nanocrystals. The screw-like feature of the nanocrystals may be due to the fact that the ligand was a chiral molecule, which dominated generally the formation of unique supramolecular aggregates or nanocrystals as having been reported by several research groups [24-26].

Secondly, the screw-like nanocrystals transformed into nanorods after the interfacial reaction time increased to about 30 min. As shown in Figure 2C,D, the length of nanorods increased to be about several micrometers with the diameters about tens of nanometers, a little increased as compared with those of the screw-like nanocrystals. This increase may be attributed to the following reasons: (1) the coordination reaction of the silver ions and bidentate ligands continued on the surface of the screw-like nanocrystals, and (2) the nanocrystals formed at the initial time were of highly active surface energy that resulted in a strong interaction between each nanocrystal. As a result, the small nanocrystals formed larger particles as those often occurred in the air-organic solvent interfaces [27].

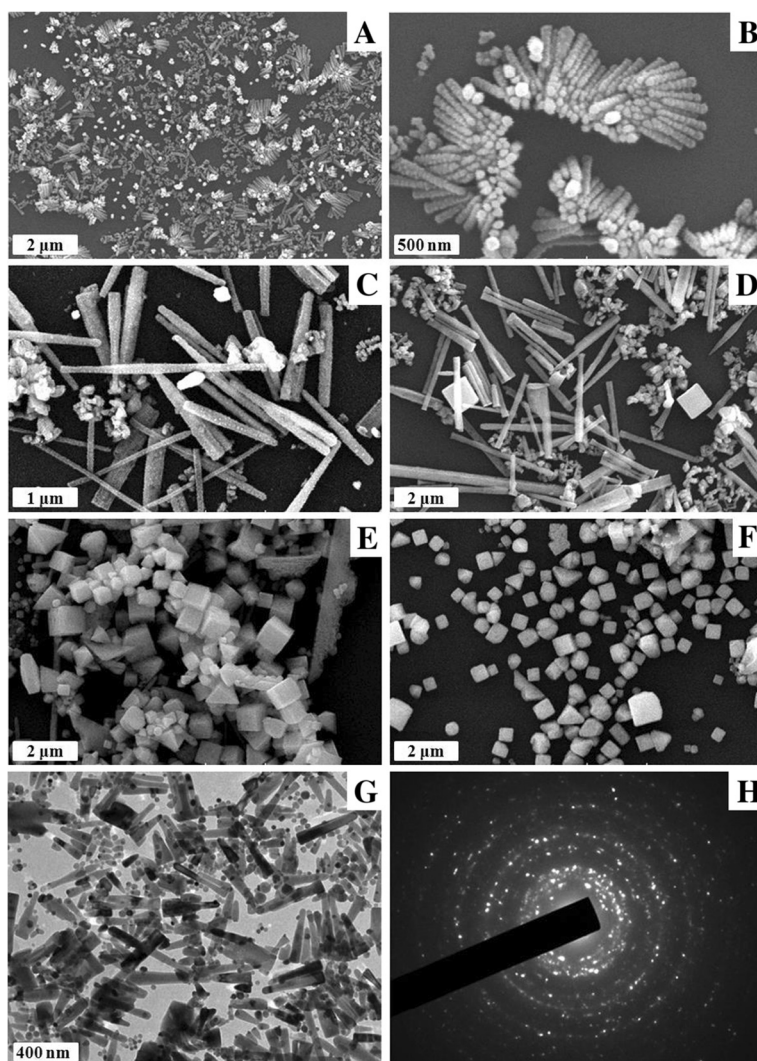


Figure 2 SEM and TEM images of $\text{Ag}(\text{DHQ})_2\text{AQN}$ nanocrystals grown at water-chloroform interface after different reaction times. SEM images after (A) 30 min, (B) 30 min (enlarged photo), (C) 2 h, (D) 12 h, (E) 3 days, and (F) 15 days; (G) TEM image after 2 h; (H) electron diffraction pattern of the nanocrystals.

Thirdly, when the interfacial reaction continued up to several days, the nanorods further grew into cubic macrocrystals with the length of a side about hundreds of nanometers (Figure 2E,F). This process was similar to that we have observed for metal-mediated nanocrystals of multiporphyrin arrays [10], wherein the shapes of the products were closely dependent on the geometries of the central metal ions. Here, the Ag^+ ions were tetrahedrally coordinated with bidentate ligand of $(\text{DHQD})_2\text{AQN}$, so screw-like or nanorods were firstly formed, then they grew into larger cubic particles. A comparison of the size of the nanorods with that of the cubic particles could further find that the cubic length was shorter than that of the nanorods; this phenomenon

may be attributed to a slow kinetic process of the crystal growing at the earlier stage, then to a thermodynamic process after several days. The other possible reason may be the lowest surface active energy of the cubic crystals; that is, the nanocubes may be more stable than the nanorods.

Similar TEM images were observed for the $\text{Ag}(\text{DHQ})_2\text{AQN}$ complex nanocrystals, but the screw-like nanocrystals formed at the initial time were not very stable under the high beam energy of TEM. As an example, Figure 2G shows a TEM photo of the Ag-complex nanocrystals at the reaction time of 2 h, which revealed that it was composed of many nanorods and dot-like aggregates and in agreement with that observed from the

SEM photos. Electron diffraction pattern of the present Ag-complex nanocrystals revealed many irregular dots (Figure 2H), indicating that they were polycrystalline.

X-ray photoelectron spectroscopy

Element compositions for the Ag-directed complex nanocrystals were detected by using the XPS technique. Also as an example, Figure 3 shows the high-resolution XPS bands for the Ag-(DHQ)₂AQN complex nanocrystals, which revealed four peaks in the binding energy from 100 to 600 eV except for the Si element from substrate surface. The binding energy of these four peaks was as follows: 284.6, 368.6/374.4, 399.4 ~ 403, and 532.6 eV, which could be assigned to the elements of C(1 s), Ag(3d), N(1 s), and O(1 s), respectively. The C, part of N, and O elements were from the ligand of (DHQ)₂AQN, while the elements of Ag, part of N, and O were from AgNO₃. Thus, these XPS data confirmed formation of Ag-(DHQ)₂AQN complex nanocrystals [20].

Absorbance and fluorescence emission of the nanocrystals

Absorption and emission features of the Ag-complex nanocrystals as-prepared were investigated on the quartz surfaces. As an example, Figure 4 shows absorption spectra for the Ag-(DHQ)₂AQN nanocrystals transferred from the water-chloroform interface at different reaction times, together with a spectrum of the ligand in the dilute methanol solution. Three absorption bands were recorded and appeared at about 230 ~ 238, 323 ~ 334, and 416 nm for the ligand of (DHQ)₂AQN in the solution, which can be designated to the electron transition of quinuclidine, quinine, and anthraquinone substituents. Our previous work has revealed that these peaks shifted to about 240, 337, and 416 nm in its Langmuir-Blodgett (LB) film [20]. When the ligand was coordinated with Ag⁺ ions to form the LB film of Ag-(DHQ)₂AQN coordination polymers,

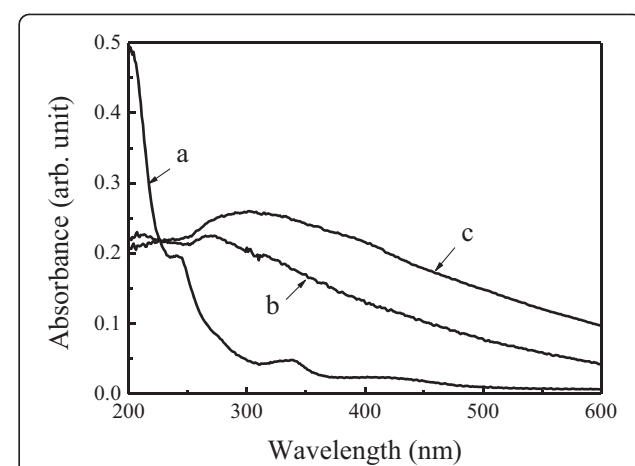


Figure 4 Absorption spectra. (a) Ligand of (DHQ)₂AQN in the methanol solution and (b) Ag-(DHQ)₂AQN nanocrystals deposited 2 h and (c) Ag-(DHQ)₂AQN nanocrystals deposited 3 days after the interfacial reaction.

these absorption bands appeared at about 245, 342, and 413 nm, respectively [20]. That is, a redshift was recorded for the former two peaks when the ligand was coordinated with Ag⁺ ions.

Here, for the films of Ag-(DHQ)₂AQN complex nanocrystals, a broad absorption band was recorded with the maximum at about 270 ~ 296 nm. But it is hard to distinguish each peak as those in the solutions and LB films [20]. This difference can be attributed to the fact that the LB film was almost transparent and did not scatter the light during the absorption measurements; however, the present film of Ag-(DHQ)₂AQN complex nanocrystals was not. The detected light was strongly scattered by the nanoparticles, resulting in a broaden band from 200 to nearly 600 nm. Moreover, with increasing the reaction time, the average sizes of the nanocrystals increased (as shown in the SEM images in Figure 2). As a result, the main absorption band a little red shifted, the feature of which was in agreement with that observed in the aggregates of inorganic complexes or macrocyclic compounds due to a strong molecular interaction in the larger aggregates or to a stronger light scattered by the larger aggregates [28,29].

Based on the chemical structure of the chiral ligands used, we can find that they contain both quinine and anthraquinone substituents, both of them are important light-harvesting units. They can not only absorb ultraviolet light but also give off emission in the near ultraviolet and visible region [30,31], so they have potential applications in the fields of optical, electroluminescent materials and light-emitting diodes. The light energy absorbed by the ligands can be further transferred to some metal ions like Eu³⁺ and Tb³⁺ as luminescent sensors, and organic light-emitting diodes [32,33]. Here, luminescent emission

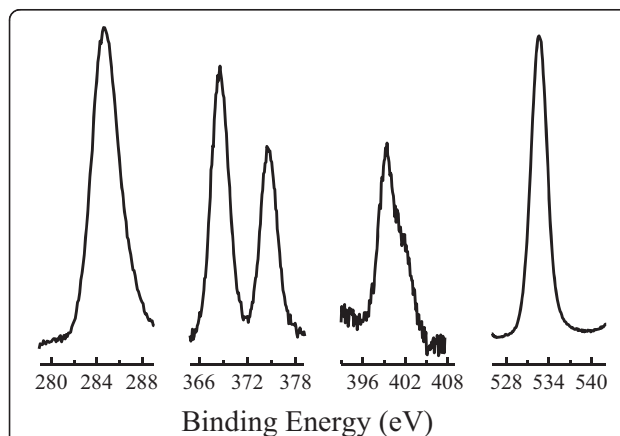


Figure 3 High-resolution XPS spectra of the Ag-(DHQ)₂AQN nanocrystals.

properties for the Ag-(DHQ)₂AQN complex nanocrystals were investigated after they were transferred on the quartz substrate surfaces.

Figure 5 shows emission spectrum for the Ag-(DHQ)₂AQN complex nanocrystals on the quartz substrate surface, together with an emission spectrum of the ligand in the methanol solution. The excited wavelength was 317 nm. These emission spectra revealed the following features. Firstly, two broad emission peaks were recorded and centered at about 363 and 520 to 530 nm for the ligand (DHQ)₂AQN in the methanol solution. The first peak may be designated to the emission from the hydroquinine substituents and the second one to that of the anthraquinone [20]. Secondly, the Ag-(DHQ)₂AQN complex nanocrystals showed also two broad emission peaks; the first one appeared at about 360 nm (very similar to that in the methanol solution), while the second one 'blue' shifted to about 470 nm. Previously, we have found that the fluorescent emission features for the ligands in the casting films were similar to those in the LB films; that is, the first one appeared at about 365 nm while the second one slightly red shifted to the range of 530 ~ 560 nm. This redshift has been attributed to a closely packed arrangement of the molecules in the organized ultrathin films as often observed for the macrocyclic molecules such as porphyrins and inorganic complexes [10-12].

The blueshift phenomenon of the second emission band was also observed in the layer-by-layer multilayers of Pd-(DHQ)₂ANQ and Pd-(DHQD)₂ANQ coordination polymers [34], which was attributed to the formation of the Pd-(DHQ)₂AQN and Pd-(DHQD)₂AQN complexes. During experiments, we measured the emission spectra for the mixtures of (DHQ)₂ANQ and AgNO₃ at the molar ratios from 1:0 to 1:10 in the methanol solution. As shown in Figure 6, the emission at approximately 360 nm did not show a significant difference with the

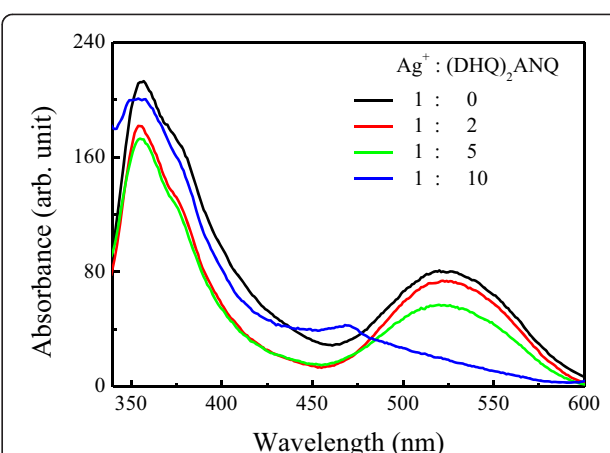


Figure 6 Fluorescence spectra for the mixtures of (DHQ)₂AQN and AgNO₃ in the methanol solutions.

increase of the relative molar fractions of AgNO₃. However, the emission at 525 nm gradually weakened when the AgNO₃ solution was added. When the molar ratios of AgNO₃ relative to the ligand increased to 10, a weak emission peak was observed at approximately 470 nm, which was in agreement with that observed in the Ag-(DHQ)₂AQN complex nanocrystals. These results suggested that the blueshift and quenching of the second emission peak may be attributed to the formation of metal-ligand complexes in the nanocrystals [34].

Voltammetric properties

Besides the interesting optical and chiral behaviors, (DHQ)₂AQN and (DHQD)₂AQN are also electroactive compounds because they contain the anthraquinone substituents, which have been widely used as electroactive materials either for the fundamental researches on electrochemistry or for the potential applications in the sensors, electrochromism, and organic batteries [32,33]. Here, the cyclic voltammograms of Ag-complex nanocrystals on the ITO electrodes were investigated and compared with those of the ligand in the casting films.

Figure 7A shows the CV curves for the ITO electrode covered by the Ag-(DHQ)₂AQN complex nanocrystals in the 0.01 mol/L HClO₄ electrolyte solutions in the potential range of -0.5 to 0 V at the scan rates from 0.05 to 0.6 V/s. One couple of redox wave was recorded with the cathodic (E_{pc}) and anodic (E_{pa}) potentials at around -0.27 ~ -0.29 and -0.22 ~ -0.20 V vs. Ag/AgCl, respectively. Based on the literature [35], this redox couple was designated to the electron transfer process of (DHQ)₂AQN and (DHQ)₂AQN⁻. The potential difference ΔE ($\Delta E = E_{pa} - E_{pc}$) was 0.05 V when the scan rate was 0.05 V/s, which slightly increased to 0.09 V when the scan rate was 0.6 V/s. The reduction current intensity was about 15.6 μ A, which was also close to that of the

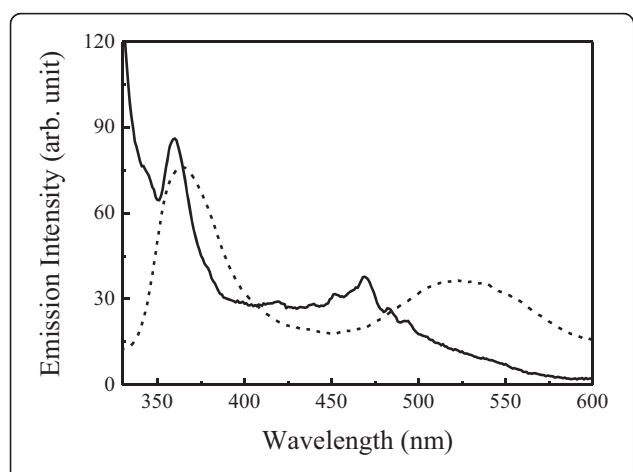
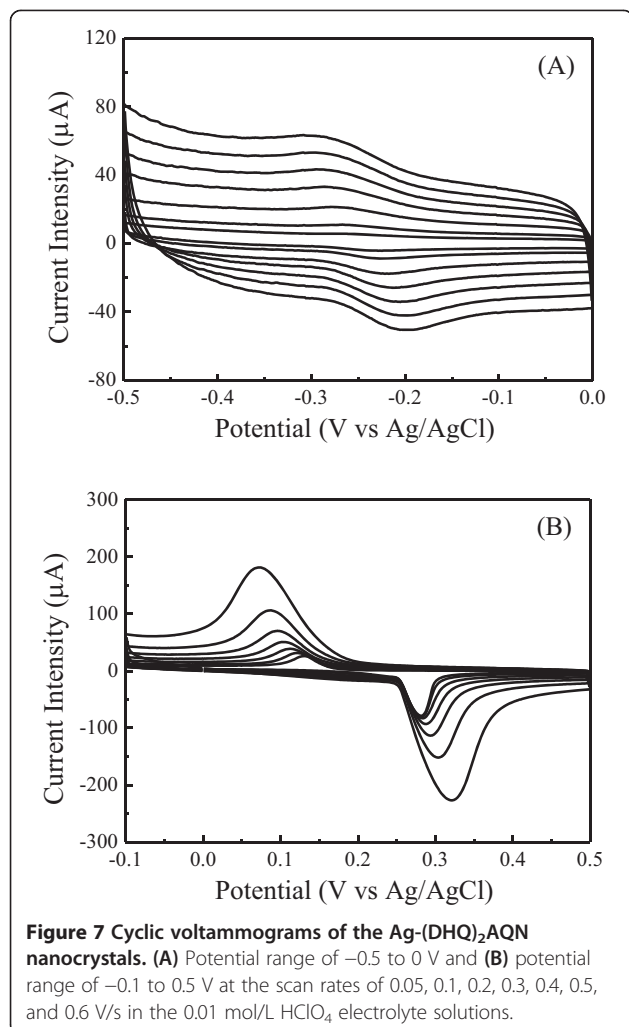


Figure 5 Fluorescence spectra. Ag-(DHQ)₂AQN nanocrystals (solid line) and the ligand in the methanol solution (dashed line).



oxidation current intensity ($12.6 \mu\text{A}$) when the scan rate was 0.6 V/s. These CV features suggested that the redox process of the ligands in the nanocrystals was reversible.

Figure 7B shows the CV curves for the $\text{Ag}-(\text{DHQ})_2\text{AQN}$ nanocrystals in the 0.01 mol/L HClO_4 electrolyte solutions in the potential range of -0.1 to 0.5 V at the scan rates from 0.05 to 0.6 V/s. One couple of redox wave was recorded with the cathodic and anodic potentials at around $-0.13 \sim 0.07$ and $0.28 \sim 0.32$ V, which was attributed to the redox reaction of the connector of Ag^+ ions [36], with the electron transfer process of $\text{Ag}-(\text{DHQ})_2\text{AQN}$ and $\text{Ag}^+-(\text{DHQ})_2\text{AQN}$. The potential difference ΔE was 0.35 V when the scan rate was 0.05 V/s, which increased to 0.45 V when the scan rate was 0.6 V/s.

Relation of the redox current intensity of the modified electrode to the scan rate and the root of the scan rate was calculated. Figure 8A shows plots of the current intensity for the reduction reaction of the ligand $\text{Ag}-(\text{DHQ})_2\text{AQN} \rightarrow \text{Ag}-(\text{DHQ})_2\text{AQN}^-$ to the scan rate and the root of the scan rate for the ITO electrode modified

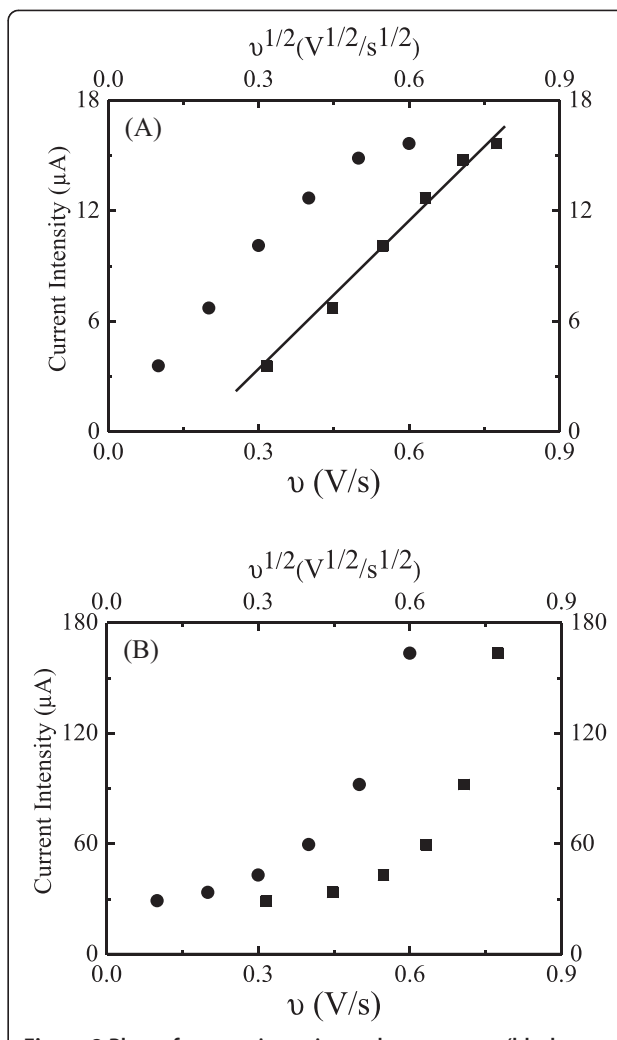


Figure 8 Plots of current intensity to the scan rates (black circles) and root of scan rates (black squares). (A) Reduction reaction of $\text{Ag}-(\text{DHQ})_2\text{AQN} \rightarrow \text{Ag}-(\text{DHQ})_2\text{AQN}^-$ and (B) reduction reaction of $\text{Ag}^+-(\text{DHQ})_2\text{AQN} \rightarrow \text{Ag}-(\text{DHQ})_2\text{AQN}$ complex nanocrystals.

by the film of $\text{Ag}-(\text{DHQ})_2\text{AQN}$ nanocrystals. Based on these data, we can find that the current intensity was proportional to the root of the scan rates rather than that of the scan rates, which indicated that the electroactive thickness of the nanocrystals was thicker than that of the diffusion layer. This was reasonable because the film was composed of irregular $\text{Ag}-(\text{DHQ})_2\text{AQN}$ complex nanocrystals with the sizes in the range of hundreds of nanometers (Figure 2). A close inspection of the figure could further find that this line did not go through the zero point. This feature suggested that, besides the diffusion layer, the electron transfer process between the $\text{Ag}-(\text{DHQ})_2\text{AQN}$ nanocrystals and electrode surface may be also influenced by some other issues, such as the interfacial resistance between the nanocrystals and electrode surface and the connectors of AgNO_3 between the ligands and electrode surface [36].

Figure 8B shows plots of the current intensity for the reduction reaction of the silver ions in the complex nanocrystals of $\text{Ag}^+ \cdot (\text{DHQ})_2\text{AQN} \rightarrow \text{Ag} \cdot (\text{DHQ})_2\text{AQN}$ to the scan rate and the root of the scan rate. Different from that observed in Figure 8A for the reduction reaction of the ligands, here, the current intensity was not proportional to neither the scan rate nor the root of the scan rate. According to the theory of film-modified electrode [37,38], this phenomenon could be attributed to that the electroactive thickness of the nanocrystals was not very thinner or very thicker as compared with that of the diffusion layer.

Conclusions

Silver(I)-directed metal-organic complex nanocrystals have been prepared using AgNO_3 as a connector and chiral bidentate ligands as linkers at the water-chloroform interface. Screw-like Ag-directed complex nanocrystals formed at the initial reaction time; then, they grew into nanorods and finally became cubic nano- or microcrystals. The as-prepared Ag-complex nanocrystals showed strong luminescent emissions as well as reversible redox properties, which may have potential interests in the fundamental researches and applications in the fields of chemically modified electrodes and optoelectronic devices.

Competing interests

The authors declare that they have no competing interests.

Authors' contributions

YT, HTW, MC, and LZ carried out the synthesis and characterizations of the materials and drafted the manuscript. ML and DJQ contributed in the design and discussion of this work and in the revision of the manuscript. All authors read and approved the final manuscript.

Acknowledgements

The authors are grateful to the National Science Foundation of China (91027042) and the Program for Changjiang Scholars and Innovative Research Team in University (IRT1117).

Author details

¹Department of Chemistry, Fudan University, 220 Handan Road, Shanghai 200433, China. ²Beijing National Laboratory for Molecular Science, CAS Key Laboratory of Colloid, Interface and Chemical Thermodynamics, Institute of Chemistry, Chinese Academy of Sciences, No. 2 Zhongguancun Beiyijie, Beijing 100190, China.

Received: 23 July 2014 Accepted: 7 September 2014

Published: 12 September 2014

References

1. Wang X, Peng Q, Li Y: Interface-mediated growth of monodispersed nanostructures. *Acc Chem Res* 2007, **40**:635–643.
2. Nikolaides MG, Bausch AR, Hsu MF, Dinsmore AD, Brenner MP, Gay C, Weitz DA: Electric-field-induced capillary attraction between like-charged particles at liquid interfaces. *Nature* 2002, **420**:299–301.
3. Jungwirth P, Finlayson-Pitts BJ, Tobias DJ: Introduction: structure and chemistry at aqueous interfaces. *Chem Rev* 2006, **106**:1137–1139.
4. Su B, Abid JP, Fermín DJ, Girault HH, Hoffmannová H, Krtík P, Samec Z: Reversible voltage-induced assembly of Au nanoparticles at liquid/liquid interfaces. *J Am Chem Soc* 2004, **126**:915–919.
5. Lin Y, Skaff H, Emrick T, Dinsmore AD, Russell TP: Nanoparticle assembly and transport at liquid-liquid interfaces. *Science* 2003, **299**:226–229.
6. Zhuov K, Dickinson EJF, Compton RG: Dynamics of ion transfer potentials at liquid-liquid interfaces: the case of multiple species. *J Phys Chem B* 2011, **115**:12429–12440.
7. Zhang SY, Liu JW, Zhang CL, Yu SH: Co-assembled thin films of Ag nanowires and functional nanoparticles at the liquid-liquid interface by shaking. *Nanoscale* 2013, **5**:4223–4229.
8. Khurana E, DeVane RH, Kohlmeyer A, Klein ML: Probing peptide nanotube self-assembly at a liquid-liquid interface with coarse-grained molecular dynamics. *Nano Lett* 2008, **8**:3626–3630.
9. Biswas S, Drzal LT: A novel approach to create a highly ordered monolayer film of graphene nanosheets at the liquid-liquid interface. *Nano Lett* 2009, **9**:167–172.
10. Liu B, Qian DJ, Huang HX, Wakayama T, Hara S, Huang W, Nakamura C, Miyake J: Controllable growth of well-defined regular multiporphyrin array nanocrystals at the water-chloroform interface. *Langmuir* 2005, **21**:5079–5084.
11. Liu B, Qian DJ, Chen M, Wakayama T, Nakamura C, Miyake J: Metal-mediated coordination polymer nanotubes of 5,10,15,20-tetrapyrrolylporphine and tris(4-pyridyl)-1,3,5-triazine at the water-chloroform interface. *Chem Commun* 2006, **30**:3175–3177.
12. Liu B, Chen M, Nakamura C, Miyake J, Qian DJ: Coordination polymer nanocombs self-assembled at the water-chloroform interface. *New J Chem* 2007, **31**:1007–1012.
13. Su K, Nuraje N, Zhang L, Chu IW, Peetz RM, Matsui H, Yang NL: Fast conductance switching in single-crystal organic nanoneedles prepared from an interfacial polymerization crystallization of 3,4-ethylenedioxythiophene. *Adv Mater* 2007, **19**:669–672.
14. Nuraje N, Su K, Yang NL, Matsui H: Liquid/liquid interfacial polymerization to grow single crystalline nanoneedles of various conducting polymers. *ACS Nano* 2008, **2**:502–506.
15. Ren ZB, Liu J, Chen YP, Chen M, Qian DJ: Facile fabrication of porous pure and Ag nanoparticle-doped poly(4-vinylpyridine) films at the liquid-liquid interfaces. *Chin Chem Lett* 2011, **22**:867–870.
16. Chen LJ, Ma H, Chen K, Cha HR, Lee YI, Qian DJ, Hao J, Liu HG: Synthesis and assembly of gold nanoparticle-doped polymer solid foam films at the liquid/liquid interface and their catalytic properties. *J Colloid Interface Sci* 2011, **362**:81–88.
17. Chu C, Yang D, Wang D, Ma H, Liu HG: Formation of Au nanoparticle-doped PVK microcapsules and foam-like structures at the liquid/liquid interface. *Mater Chem Phys* 2012, **132**:916–922.
18. Chu C, Wang D, Ma H, Yu M, Hao J, Liu HG: Assembly of foam and honeycomb films of a diblock copolymer doped with Au or Ag nanoparticles at the liquid/liquid interface and their catalytic properties. *Mater Chem Phys* 2013, **142**:259–267.
19. Ma H, Geng Y, Lee YI, Hao J, Liu HG: Free-standing poly(2-vinylpyridine) foam films doped with silver nanoparticles formed at the planar liquid/liquid interface. *J Colloid Interface Sci* 2013, **201**:223–230.
20. Tang Y, Chen M, Qian DJ, Zhang L, Liu M: Interfacial self-assembly and characterization of chiral coordination polymer multilayers with bidentate ligands of hydroquinine anthraquinone-1,4-diyl diether as linkers. *Langmuir* 2013, **29**:6308–6316.
21. Rao CNR, Kulkarni GU, Agrawal W, Gautam UK, Ghosh M, Tumkurkar U: Use of the liquid-liquid interface for generating ultrathin nanocrystalline films of metals, chalcogenides, and oxides. *J Colloid Interface Sci* 2005, **289**:305–318.
22. Milliron DJ, Buonsanti R, Llordés A, Helms BA: Constructing functional mesostructured materials from colloidal nanocrystal building blocks. *Acc Chem Res* 2014, **47**:236–246.
23. Khlobystov AN, Blake AJ, Champness NR, Lemenovskii DA, Majouga AG, Zykov NV, Schröder M: Supramolecular design of one-dimensional coordination polymers based on silver(I) complexes of aromatic nitrogen-donor ligands. *Coord Chem Rev* 2001, **222**:155–192.
24. Schmuck C: Molecules with helical structure: how to build a molecular spiral staircase. *Angew Chem Int Ed* 2003, **42**:2448–2452.
25. Fan Z, Govorov AO: Chiral nanocrystals: plasmonic spectra and circular dichroism. *Nano Lett* 2012, **12**:3283–3289.
26. Shen X, Asenjo-García A, Liu Q, Jiang Q, Abajo FJG, Liu N, Ding B: Three-dimensional plasmonic chiral tetramers assembled by DNA origami. *Nano Lett* 2013, **13**:2128–2133.
27. Pilani MP: Supra- and nanocrystallinity: specific properties related to crystal growth mechanisms and nanocrystallinity. *Acc Chem Res* 2012, **45**:1965–1972.

28. Chan LMW, Tischler JR, Kooi SE, Bulović V, Swager TM: **Synthesis of J-aggregating dibenz[a, j]anthracene-based macrocycles.** *J Am Chem Soc* 2009, **131**:5659–5666.
29. McCarthy BD, Hontz ER, Yost SR, Voorhis TV, Dincă M: **Charge transfer or J-coupling assignment of an unexpected red-shifted absorption band in a naphthalenediimide-based metal-organic framework.** *J Phys Chem Lett* 2013, **4**:453–458.
30. Batista RMF, Oliveira E, Costa SPG, Lodeiro C, Raposo MMM: **Cyanide and fluoride colorimetric sensing by novel imidazo-anthraquinones functionalised with indole and carbazole.** *Supramol Chem* 2014, **26**:71–80.
31. Joshi S, Varma YT, Pant DD: **Steady state and time-resolved fluorescence spectroscopy of quinine sulfate dication in ionic and neutral micelles: effect of micellar charge on photophysics.** *Colloids Surf A: Physicochem Eng Aspects* 2013, **425**:59–67.
32. Rao X, Huang Q, Yang X, Cui Y, Yang Y, Wu C, Chen B, Qian G: **Color tunable and white light emitting Tb³⁺ and Eu³⁺ doped lanthanide metal-organic framework materials.** *J Mater Chem* 2012, **22**:3210–3214.
33. Chelebaeva E, Long J, Larionova J, Ferreira RAS, Carlos LD, Almeida Paz FA, Gomes JBR, Trifonov A, Guérin C, Guari Y: **Bifunctional mixed-lanthanide cyano-bridged coordination polymers Ln_{0.5}Ln'_{0.5}(H₂O)₅[W(CN)₈] (Ln/Ln' = Eu³⁺/Tb³⁺, Eu³⁺/Gd³⁺, Tb³⁺/Sm³⁺).** *Inorg Chem* 2012, **51**:9005–9016.
34. Tang Y, Chen M, Qian DJ, Zhang L, Liu M: **Palladium(II)-directed layer-by-layer assembly of chiralmetal-organic complex multilayers with bidentate ligands of hydroquinine anthraquinone-1,4-diyli diether as linkers on substrate surfaces.** *Colloids Surf A: Physicochem Eng Aspects* 2014, **457**:41–48.
35. Oyaizu K, Choi W, Nishide H: **Functionalization of poly(4-chloromethylstyrene) with anthraquinone pendants for organic anode-active materials.** *Polym Adv Technol* 2011, **22**:1242–1247.
36. Sun Q, Liu J, Huang HX, Chen M, Qian DJ: **Self-assembled monolayers of pyridylthio-functionalized carbon nanotubes used as a support to immobilize cytochrome c.** *Nanoscale Res Lett* 2013, **8**:63.
37. Dong SJ, Che GL, Xie YW: *Chemically Modified Electrodes*. Beijing: Chinese Science Press; 1995:52–63.
38. Murray RF: In *Electrochemical Chemistry*, Volume Volume 13. Edited by Bard AJ. New York: Marcel Dekker Press; 1984:191.

doi:10.1186/1556-276X-9-488

Cite this article as: Tang et al.: Silver(I)-directed growth of metal-organic complex nanocrystals with bidentate ligands of hydroquinine anthraquinone-1,4-diyli diethers as linkers at the water-chloroform interface. *Nanoscale Research Letters* 2014 **9**:488.

Submit your manuscript to a SpringerOpen® journal and benefit from:

- Convenient online submission
- Rigorous peer review
- Immediate publication on acceptance
- Open access: articles freely available online
- High visibility within the field
- Retaining the copyright to your article

Submit your next manuscript at ► springeropen.com